Title	Effects of aspect-ratio on the flapping behaviour of energy-harvesting membrane
Author(s)	Shi, Shengxian.; New, T. H.; Liu, Yingzheng.
Citation	Shi, S., New, T.H., & Liu, Y. (2014). Experimental Thermal and Fluid Science. Effects of aspect-ratio on the flapping behaviour of energy-harvesting membrane, 52, 339-346.
Date	2013
URL	http://hdl.handle.net/10220/16765
Rights	© 2013 Elsevier Inc. This is the author created version of a work that has been peer reviewed and accepted for publication by Experimental Thermal and Fluid Science, Elsevier. It incorporates referee's comments but changes resulting from the publishing process, such as copyediting, structural formatting, may not be reflected in this document. The published version is available at: [http://dx.doi.org/10.1016/j.expthermflusci.2013.09.014].

Effects of aspect-ratio on the flapping behaviour of energy-harvesting membrane

Shengxian Shi[1], T. H. New[2] and Yingzheng Liu[1*]

[1]Key Laboratory for Power Machinery and Engineering of Ministry of Education, School of Mechanical Engineering, Shanghai Jiao Tong University, 200240, Shanghai, China

[2]School of Mechanical and Aerospace Engineering, Nanyang Technological University, 50 Nanyang Avenue, Singapore 639798, Singapore

Abstract

Experimental studies were carried out on aspect-ratios of 2 and 3 rectangular polyethylene terephthalate membranes to clarify the effects of aspect-ratio on membrane flapping dynamics and strain energy distribution for Reynolds numbers from 3228 to 9732. Flapping modes similar to our previous study are identified and an increase in aspect-ratio is observed to promote transition of membrane flapping from limited cantilever-like mode to quasi-periodical travelling wave mode. This leads to corresponding increases in the flapping amplitude and its growth rate. On the other hand, both membranes achieve "lock-in" states at the same Reynolds number with nearly identical flapping frequency growth rates. Increasing the membrane aspect-ratio leads to strong variations in the strain distributions and reduces its increments with the Reynolds number Lastly, estimated membrane strain energy increases more with the Reynolds number for the higher aspect-ratio membrane. Compared to the lower aspect-ratio membrane however, it reaches an asymptotic level once it attains "lock-in" condition due to the more three-dimensional flapping motions.

Keywords: Flexible membrane; Flapping dynamics; Energy harvesting; Vortex-membrane interaction

* Corresponding author
E-mail address: yzliu@sjtu.edu.cn

1. Introduction

Flexible piezoelectric polyvinylidene fluoride (PVDF) membranes are able to flap continuously by subjecting themselves to regular impingement of wake vortices shed by a bluff body positioned upstream under certain conditions (i.e. membrane aspect-ratio, bluff body size and free stream velocity, take for instance). As such, useful electric energy can be generated from the mechanical strain energy incurred in deformed PVDF membranes. Some of the earliest studies on the use of flapping PVDF membranes (also known as energy harvesting eel) were carried out by Allen and Smits [1] and Techet et al. [2], which demonstrated that relatively large aspect-ratio PVDF membranes are able to couple well with the wake vortices and flap at close to the actual vortex-shedding frequency when located downstream of a blunt flat plate. Similar studies were also performed by Taylor et al. [3] and Pobering et al. [4], though their emphasis was more on the theoretical analysis of membrane harvesting system, circuit optimisation and electrical power output measurements. Besides the energy harvesting eel method, piezoelectric cantilever, ionic polymer metal composites, elastic slender structures and sonic crystal and the piezoelectric material were also applied to harvest fluidic energy through flow induced vibration and aeroelastic vibrations. Detailed review on these techniques will not be given here as it will deviate from the current topic. For the latest progress on these researches as well as other energy harvesting methods, interested readers are referred to Elvin and Erturk [5].

Although preceding studies had demonstrated the feasibility of using flexible PVDF membranes to harvest fluid kinetic energy from bluff body wake vortices, there exist further needs to improve our understanding in terms of the fluid-structure coupling between the membranes and wake vortices. In particular, better appreciation of the effects conferred by the bluff body and

membrane geometries are the very first steps toward improving membrane energy-harvesting efficiency. To that end, the authors had conducted an earlier investigation on the flapping dynamics of low aspect-ratio flexible membranes (Shi et al. [6]). The study revealed that a low aspect-ratio of AR=1.67 flexible polyethylene terephthalate (PET) membrane was able to exhibit three different flapping modes for Reynolds numbers ranging between Re=3200 to 12000 and that frequency "lock-in" phenomenon existed, even though it occurred at a Reynolds number quite different from that observed by Allen and Smits [1] previously.

From the fluids dynamics perspective, it is clear from the authors' earlier study that the membrane aspect-ratio exerts significant influences upon the overall flapping response of membrane to wake vortices impingements. On the other hand, from the perspectives of practical implementation, exceedingly high aspect-ratio membranes may face issues associated with interferences and entanglements with their neighbours if a membrane array configuration was employed, as well as pronounced loss of coherency in the wake vortices due to three-dimensional effects (Techet et al. [2]). Therefore, there should be a range of optimal membrane aspect-ratio whereby detrimental effects can be mitigated, while energy harvesting is optimised. Hence, this study is motivated by the desire to clarify the effects of varying the membrane aspect-ratio and to extend the understanding derived from the earlier study on a comparatively lower aspect-ratio of AR=1.67 membrane. To do this, the present study explored the use of aspect-ratios of AR=2 and 3 flexible membranes located in the wake of a square cylinder. Furthermore, similar evaluation metrics will be used here to assess the differences in the flapping behaviour of AR=2 and 3 membranes and the resulting mechanical strain energy induced in them, so as to ease comparisons.

2. Experimental setup and procedures

(a) Water tunnel, cylinder and test membranes

As the experimental procedures adopted here were relatively similar to those utilised by Shi et al. [6], only the differences will be presented for the sake of brevity. For the purpose of the present study, a low-speed recirculating water tunnel at the School of Mechanical and Aerospace Engineering, Nanyang Technological University Singapore was utilised. The test section size measured approximately 450mm (W) × 600mm (H) × 1500mm (L) and the maximum free-stream turbulence level was no greater than approximately 2% of the free-stream velocities used. Free stream velocity was varied between U=0.05m/s to 0.16m/s in the present investigation.

Figure 1 shows the schematic of the experimental setup. A square cylinder measured 60mm (D) × 60mm (D) × 300mm (H) was installed vertically in the centre of water tunnel test section at zero angle-of-incidence to the free-stream direction. Flow Reynolds number based on cylinder dimensions hence ranged between Re_D=3228 to 9732. Note that this Reynolds number range came close to that used in the earlier study. Regardless of the aspect-ratio, PET membranes were installed in the wake region of the square cylinder along its centreline, which was aligned with the streamwise centreline of the water tunnel test section. The membrane was positioned 60mm (i.e. 1D) downstream of the cylinder by having its entire leading-edge attached firmly onto a 2mm diameter stainless steel rod fixture. This fixture was shaped such that it attached back to the square cylinder again.

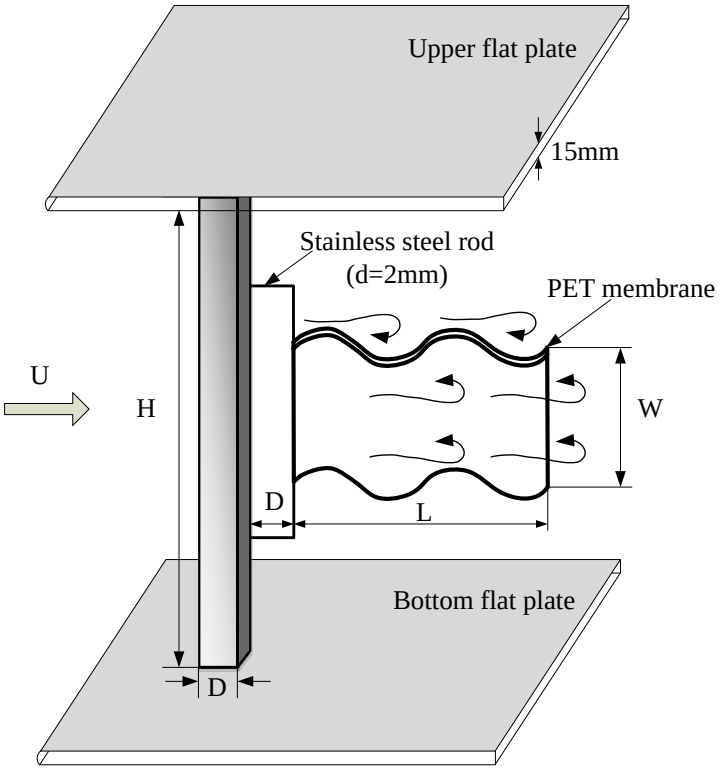

Fig. 1 Schematics of the experimental apparatus

Since the present study represents a follow-up study to our earlier study, similar PET based membranes were used. This material is transparent and offered excellent light access during the imaging experiments. Furthermore, Young's modulus of PET material ($E_{PET}=2.0\times10^9 N/m^2$ [7]) was reasonably close to that of PVDF material ($E_{PVDF}=2.24\times10^9 N/m^2$ [1]), which indicated that the flapping behaviour of PET and PVDF membranes should be generally comparable. For the AR=2 and 3 PET membranes, they had physical dimensions of 100mm (W) × 200mm (L) and 100mm (W) × 300mm (L) respectively with a uniform thickness of 0.1mm. The entire cylinder-membrane setup was positioned between two similar 15mm thickness flat plates with round leading-edges and a separation distance of 300mm to minimise any free-surface effects on the membrane flapping behaviour. Due to the 100mm width of the membranes, the distances between the membrane from either one of the flat plates was maintained at 100mm throughout.

(b) Imaging and post-processing procedures

To investigate the membrane flapping dynamics quantitatively in similar fashion as Shi et al. [6], physical outlines of the flapping membranes were recorded by an 8-bit grayscale, 1280pixel ×1024pixel Fastec Imaging HiSpec-1 camera with a Nikon f2.8 28mm lens at 15 frames-per-second (fps) with illumination provided by a Halogen lamp. The camera was installed below the bottom glass wall of the water tunnel to capture the membrane bottom edges. The resulting image spatial resolution was approximately 0.23mm/pixel. It should be noted that significant three-dimensionalities existed in the flapping motions of the two PET membrane from Re_D=6234 onwards. Therefore, for the sake of consistency, outlines of the membrane bottom edges, rather than those along the membrane mid-width, were recorded throughout this study.

Illuminating the membrane mid-width using a thin laser sheet produced by a 3W, 532nm wavelength, continuous-wave diode-pumped solid state laser from Coherent Inc. and capturing the illuminated outlines were attempted. However, severe internal light reflections within the transparent membranes due to even mild three-dimensional flapping behaviour caused the entire membrane to be internally illuminated instead. It has to be acknowledged here that outlines of the membrane bottom edge would not best represent the flapping motion of the entire membrane at higher Reynolds numbers. However, for comparisons between the two membranes studied within the present investigation, this experimental limitation was deemed to be acceptable. Vortex shedding frequencies across the tested Reynolds number were estimated from the images captured and estimated to be approximately f_v=0.12 to 0.37Hz. These frequencies corresponded to Strouhal numbers of approximately St_D=0.13 to 0.14. Despite having a membrane attached at the cylinder downstream location, these vortex shedding frequencies came close to the Strouhal

number measured by Okajima [8] for square cylinders, which was about St_D=0.13. Based on the vortex-shedding frequencies, the 15fps image-capturing rate was sufficiently fast to resolve accurately the membrane flapping motions.

A total of 11,438 sequential image frames were captured at each Reynolds number for each membrane to allow statistically meaningful analysis for the membrane flapping motions. The membrane image sequences were processed with the same technique as the earlier study, where membrane outlines were discretely identified using "Texton" algorithm (Jeon et al. [9]), before they were fitted to 10th-order polynomial equations to digitally reconstruct back the membrane outlines. Lastly, to extract information upon the dominant flapping motions, Proper Orthogonal Decomposition (POD) was used on the time-sequenced reconstructed membrane outlines. For more details, readers are referred to the earlier study for a fuller description of the image processing procedures.

3. Results and discussions

(a) Flapping dynamics and characteristics

Visual inspection of the time-sequenced membrane images revealed that AR=2 and 3 membranes responded quite differently to the wake vortices shed by the square cylinder across the entire Reynolds number range tested here. However, to have a more accurate assessment of the differences in flapping behaviour not only between the two membranes, but across different Reynolds numbers, results from POD analysis were used to classify the flapping behaviour at each test configuration according to the modes identified by the authors in their earlier study. In that study, three different dominant flapping modes were found: Mode A where limited

cantilever-like oscillations of the membrane exist, Mode B where the flapping behaviour comprises of combinations of limited cantilever-like oscillations and travelling waves, and Mode C where the flapping behaviour resembles quasi-periodical travelling waves.

Based on the above definitions, typical flapping membrane outlines and the Reynolds number ranges associated with the three different flapping modes observed in AR=2 and 3 membranes are shown in Fig. 2. To demonstrate that the flapping modes are indeed distinctively divided into Modes A, B and C for both membranes, instantaneous membrane outlines associated with flapping behaviour at three different Reynolds numbers for each membrane are presented in Figs. 2(a) and 2(c). It can be readily discerned that they agree well with the three different modes. However, it can also be observed that the Reynolds number ranges for Modes A, B and C are affected by the different membrane aspect-ratios. Take AR=2 membrane for instance, Modes A, B and C occur between Re_D=3228 to 4716, Re_D=5244 to 6756 and Re_D=7188 to 9732 respectively. As for AR=3 membrane, they occur between Re_D=3228 and 3630, Re_D=4260 and Re_D=4716 to 9732 respectively instead. These observations are in good agreement with observations made by Allen and Smits [1], where two distinct flapping modes termed as “rigid splitter-plate” and “traveling waveform” modes [i.e. corresponding to Modes A and B here] were reported for a Reynolds number range of Re_D=5000 to 40000.

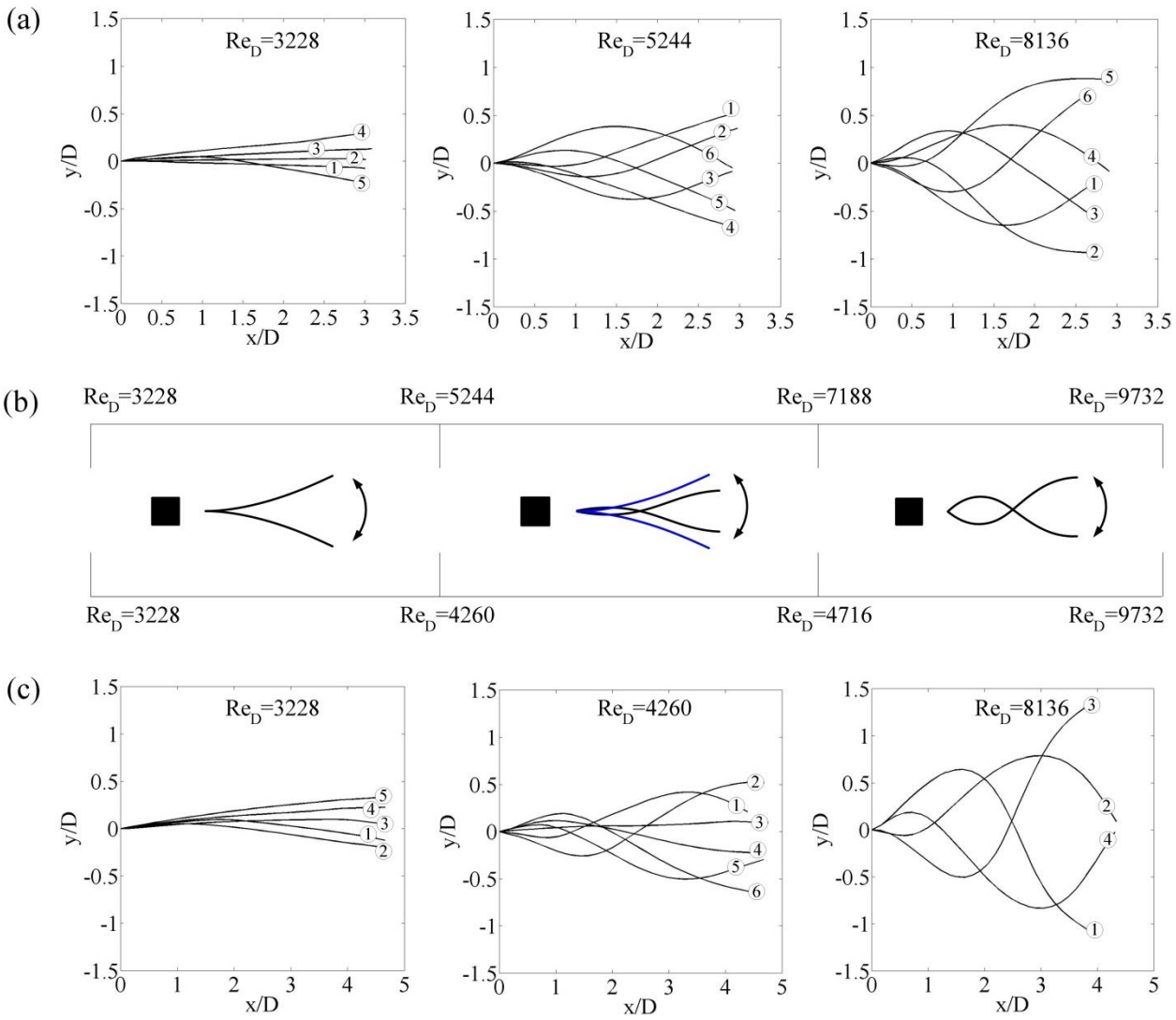

Fig.2 Typical sequence of membrane outlines at various Reynolds numbers for (a) AR=2 and (c) AR=3 membranes and (b) the dominant flapping outlines for two aspect ratio cases

Comparing between AR=2 and 3 membranes here, it is interesting to note that mode transitions occur consistently at lower Reynolds numbers for the higher aspect-ratio membrane. As a result, there is a significant increase in the Reynolds number range for Mode C as the aspect-ratio increases, at least for the conditions employed in the present study. Since Mode C is associated with the most rigorous form of flapping behaviour here, it is clear that lower structural stiffness of higher aspect-ratio membranes allow them to respond better to wake vortices impinging upon

them. This notion is supported qualitatively upon closer inspection of Fig. 2(a) and 2(c), where the membrane outlines appear to incur larger flapping amplitudes for the AR=3 membrane. On the other hand, the reduced effective stiffness would more easily induce three-dimensional flapping motions, especially at higher Reynolds numbers.

To qualitatively present the effect of aspect-ratio on the nature of the flapping motions, a cycle of membrane outline frames was shown in Fig. 3 and 4 for AR=2 and 3 membranes at ReD=9732 respectively. Two video clips were also provided for a clearer appreciation of the three-dimensional motions. To ease comparisons, images were presented at the same scale for both membranes. As shown in Fig. 3, the AR=2 membrane flapping motion is generally two-dimensional, i.e. the bottom edge (highlighted in red dotted line) is nearly parallel to the top edge (highlighted in white dotted line). On the other hand, significantly more three-dimensional motions are observed for the AR=3 membrane at this Reynolds number. This can be discerned clearly from Fig. 4, where strong twisting of the membrane by the flow field can be seen at 0T, 1/6T, 3/6T, 4/6T and 5/6T (T stands for one flapping cycle). The severe three-dimensional motions incurred by the AR=3 membrane would inevitably reduce the strain occurred near the membrane trailing edge, and eventually lead to a saturation of the overall energy harvested from the wake vortices.

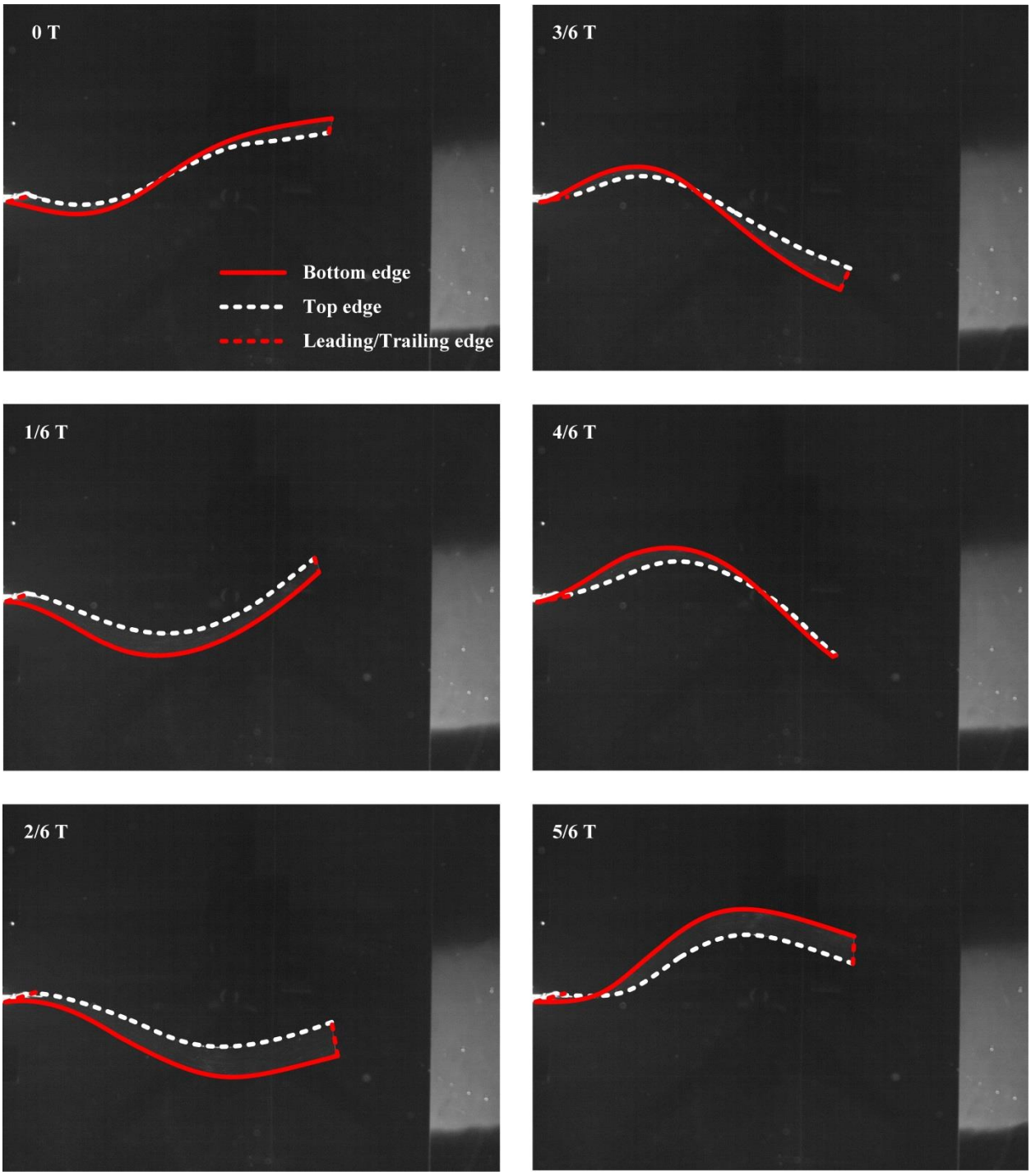

Fig. 3 Flapping motion associated with the AR=2 membrane at Re_D=9732

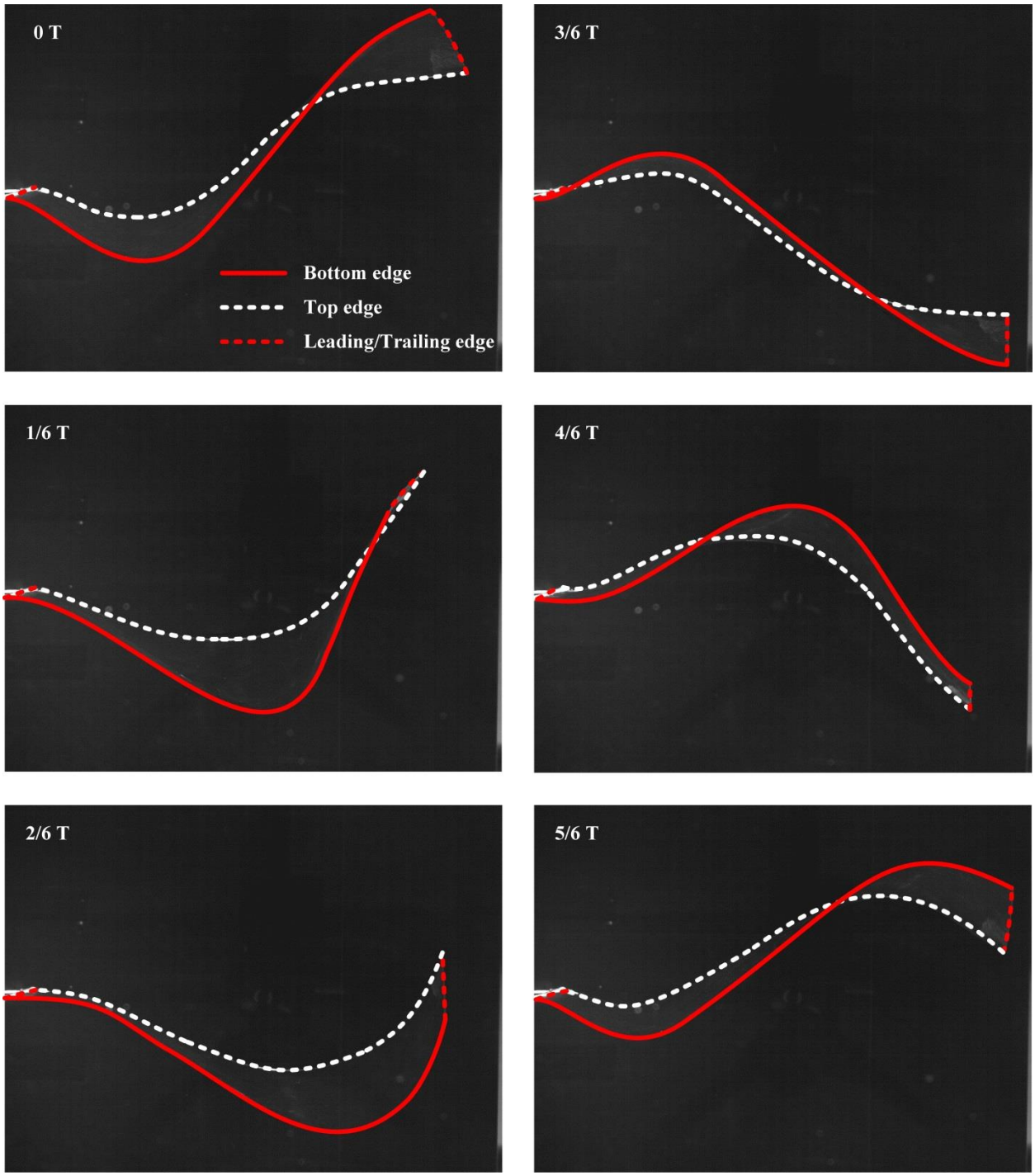

Fig. 4 Flapping motion associated with the AR=3 membrane at Re_D=9732

To look at the flapping amplitude in greater details, these membrane outlines will be analysed quantitatively. To accomplish that, tip-deflections of all instantaneous membrane outlines reconstructed from each test configuration were extracted. Using similar definitions as Allen and Smits [1] and Shi et al. [6], membrane flapping amplitude (A) is defined as the maximum tip-to-tip deflection of the membrane trailing-edge derived from the 11,438 membrane outlines. At the same time, flapping frequencies were determined by performing a Fast Fourier Transform (FFT) on the time-sequenced membrane outline data as well. Similar to Shi et al. [6], FFT calculations were performed at four different streamwise locations along the length of the membrane (i.e. x/L=0.2, 0.4, 0.6 and 0.8, where x and L are the streamwise distance from the membrane leading-edge and membrane length respectively) to verify the independence of flapping frequency on the calculation location. Once that had been ascertained, the flapping frequencies were determined at a fixed location of x/L=0.6 for all test configurations.

The results are shown in Fig. 5, where normalised flapping amplitudes and flapping frequencies for AR=2 and 3 membranes are plotted against Reynolds numbers. With reference to Fig. 5(a), the normalised flapping amplitude generally increases with Reynolds number, which agrees well with results reported by Allen and Smits [1] and Shi et al. [6] earlier. More importantly, the same figure shows that for the same Reynolds number, the flapping amplitude increases with membrane aspect-ratio. Furthermore, its growth rate with respect to Reynolds number increases with the membrane aspect-ratio as well. These two observations confirms the earlier notion that increasing the membrane aspect-ratio will effectively increase the membrane overall flexibility

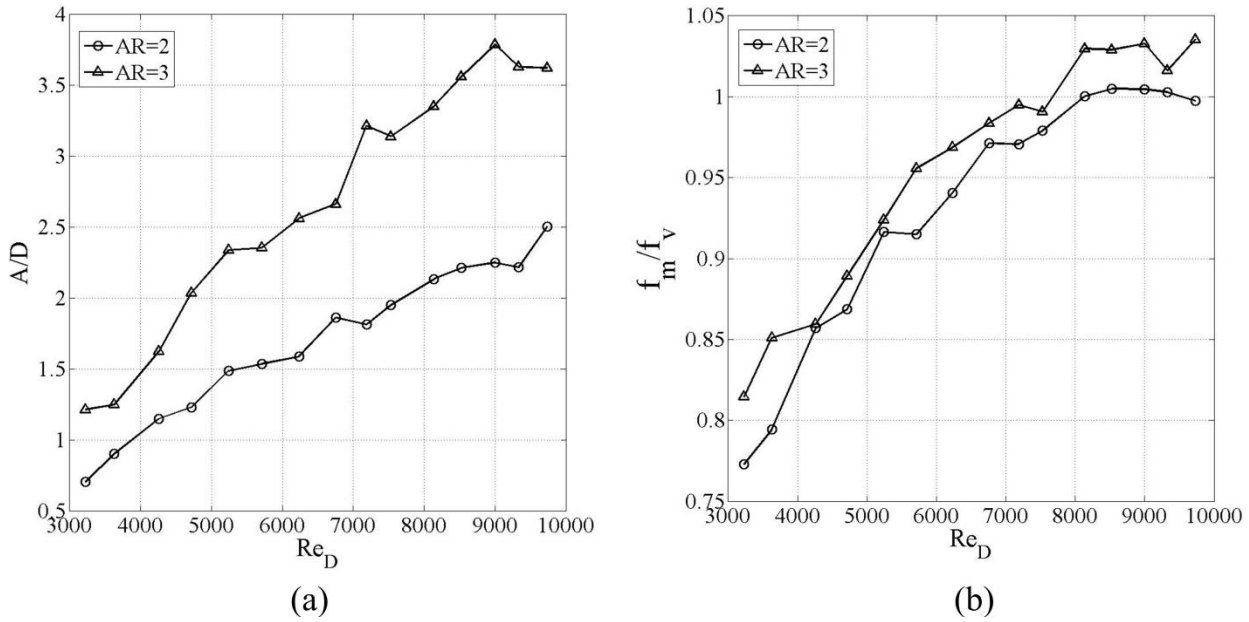

Fig. 5 Variations of (a) maximum flapping amplitudes and (b) flapping frequencies with Reynolds numbers for AR=2 and 3 membranes

and its ability to couple well with the wake vortices.

As for flapping frequencies shown in Fig. 5(b), they can be used to evaluate how well a membrane couples with the wake vortices. As pointed out by Allen and Smits [1], Techet et al. [2] and Shi et al.[6], optimal coupling between a membrane and wake vortices occurs when the membrane flapping frequency, f_m, comes very close to the vortex-shedding frequency, f_v. In fact, the membrane is considered to exhibit a "lock-in" phenomenon when the normalised flapping frequency-ratio reaches unity (i.e. $f_m/ f_v=1$), where the membrane is continuously deformed by wake vortices and undergo a periodic traveling-waveform like flapping motion. At this point, energy-harvesting will be considered as optimal and can be used as one of the key criterion to evaluate the effectiveness of cylinder-membrane setup as an energy-harvesting device.

Returning to Fig. 5 (b), it can be discerned that AR=3 membrane consistently attain slightly higher frequency-ratios than the AR=2 membrane at the same Reynolds number. However, the overall growth rates of their frequency-ratio are nearly the same, which indicates that while increasing the membrane aspect-ratio from AR=2 to 3 mildly improves its coupling with the wake vortices, the Reynolds number plays a more dominant role. In fact, this observation is not limited to relatively low aspect-ratio membranes studied here. Similar observations were also made by Allen and Smits [1] for large aspect-ratio membranes. In their study, the flapping frequencies of the AR=8 and AR=6 PVDF membranes were identical when they were both placed in the wake of a 1.5in wide plate, whereas the flapping frequency growth rate of the AR=8 PVDF membrane was larger when it was installed in the wake of a 2in wide plate.

The discrepancy in the frequency growth rate observed in Allen and Smits [1] can be attributed to two possible reasons: Firstly, larger-scale and stronger wake vortices shed by the larger 2in wide plate are likely to incur larger membrane deformations and promotes better fluid-structure coupling. This is in contrast to smaller-scale wake vortices which occasionally may not be sufficiently energetic to deform the membrane that well. Secondly, as mentioned earlier, a higher aspect-ratio membrane is structurally less resistant towards deformation by the wake vortices. Therefore, similar to the present study, past observations support the notion that, other than the nature of the wake vortices produced by the upstream bluff body, the aspect-ratio also plays an important role in the state of fluid-structure coupling between the membrane and wake vortices.

(b) Energy-harvesting predictions

Piezoelectric PVDF membranes will generate electric energy when they are deformed, where the energy production level is proportional to the mechanical strain energy built-up by the membrane under various states of deformation during the flapping motions. In this section, strain distribution along the membrane length and total strain energy incurred by the whole membrane at each Reynolds number tested will be determined using similar procedures as the previous study, for the sake of consistency. Note that conversion of strain energy into electric energy depends not only upon the piezoelectric material properties, but also on the electrical energy-extraction circuit used. However, the latter will not be considered here since the electrical energy-extraction circuit can be quite varied from case to case with different energy-extraction efficiencies. These results will provide additional insights not only into the distributions of electrical energy production along different parts of the membrane, but also allow more direct comparisons of the maximum possible energy production between different membranes.

As the PET membranes used in the current study do not generate electrical power as PVDF membranes do, their strain energy distributions were predicted based on the Young's modulus for PVDF material due to its close value to that of PET material. Firstly, the strain, ε, at all membrane locations was determined according to the following equation for every time sequenced membrane outline (Techet et al. [2]). Where h is the membrane thickness and R is the curvature.

$$\varepsilon = hR/2 \qquad (1)$$

Mean strain distributions for three representative Reynolds numbers were then averaged over 11,438 instantaneous strain distributions. Note that due to the nature of flapping where the

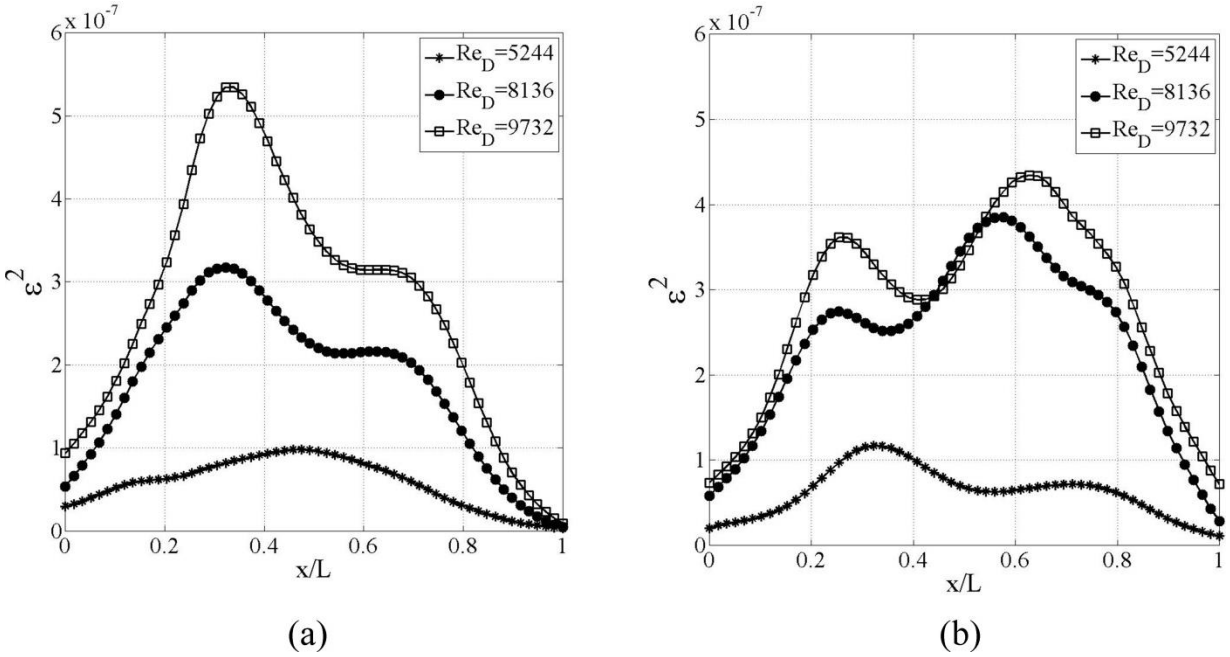

Fig. 6 Squared-strain distributions along the membrane length for
(a) AR=2 and (b) AR=3 membranes

membrane can deform towards either of its sides, instantaneous strain data were squared before taking the average (Fig. 6). For both of the membranes, the three selected Reynolds number are Re_D=5244 (i.e. prior to "lock-in" state where $f_m/f_v<1$), 8136 (i.e. at "lock-in" state where $f_m/f_v\approx1$) and 9732 (i.e. post "lock-in" where $f_m/f_v<1$).

It can be seen from Fig. 6(a) that for the AR=2 membrane, overall strain distributions are non-uniform along the entire membrane length, particularly more so as the Reynolds number increases with significant increments in their magnitudes. Note that the case prior to "lock-in" state (i.e. Re_D=5244) has only one strain peak existing at approximately x/L=0.5 location. This is due to the fact that this membrane incurs Mode B flapping (i.e. limited cantilever-like oscillations and travelling waves) at this Reynolds number and maximum deformation occurs mostly in the middle of the membrane. In contrast, two strain peaks are located at approximately

x/L=0.3 and 0.7 respectively at and post "lock-in" states (i.e. Re_D=8136 and 9732 respectively), where the membrane exhibits Mode C flapping (i.e. quasi-periodical travelling waves). Note that the first strain peak has a significantly higher magnitude than the second strain peak. These results are in good agreement with the earlier study by the authors on an AR=1.67 membrane.

On the other hand, strain distributions for the AR=3 membrane as shown in Fig. 6(b) are quite different from its AR=2 counterpart, even if the strain distributions remain non-uniform along the membrane length and overall magnitude increases with Reynolds number. Firstly, the membrane prior to "lock-in" state (i.e. Re_D=5244) has two strain peaks approximately located at x/L=0.3 and 0.7 as well. Recall that the AR=3 membrane exhibits Mode C flapping at Re_D=5244 whereas its AR=2 counterpart exhibits Mode B flapping, and that three dimensional flapping effect is moderate at this Reynolds number. Therefore, it is unsurprising that the AR=3 membrane has higher strain than its AR=2 counterpart at this point. Secondly, the increase in strain magnitudes as the AR=3 membranes transit from its "lock-in" state to post "lock-in" state is not as pronounced as the case for AR=2 membrane. This is likely due to the fact that membrane flapping motions are more three-dimensional at higher Reynolds numbers for the AR=3 membrane, due to deteriorations in the coherence level of the wake vortices as they travelled along a physically longer membrane. The increased three-dimensionalities would result in comparatively smaller membrane deformations and reduced strain levels. Thirdly, the first strain peak now has a lower magnitude compared to the second strain peak. Notice also that the magnitude discrepancy between the higher and lower strain peak is also smaller now. Collating the flapping sequences of AR=2 and 3 membranes at Re_D=8136 (i.e. the membrane outlines numbered 2, 5 in Fig. 2(a) and those numbered 2, 4 in Fig. 2(c)), it can be observed that the

second peak/valley of the travelling wave becomes dominant with an increase in the physical membrane length. As a result, this contributes towards and explains the higher magnitudes associated with the second strain peak, closer to the membrane trailing-edge. Lastly, there is a small but nonetheless upstream shift in the strain peak locations along the membrane length for AR=3 membrane. These findings are surprising as results shown earlier in Figs. 2 and 5 tend to suggest more gradual changes when the membrane aspect-ratio increases from AR=2 to 3. While the exact reasons remain unclear to the authors, it is plausible that significant increase in three-dimensional flow and hence flapping behaviour (Fig. 4) is responsible.

Compared to Techet et al. [2], high strain levels tend to occur further away from the membrane leading- and trailing-edges when the aspect-ratio is low, at least for the AR=1.67 investigated earlier in Shi et al. [6] and the AR=2 and 3 membranes tested here. In contrast, results from Techet et al. [2] show that high strain levels exist further upstream for high aspect-ratio membranes. Upon closer inspection, it was revealed that they made use of a freely-swivelling hinge to attach the membranes. In contrast, the membranes here were attached to a non-swivelling hinge. As such, it would be more difficult for the wake vortices to deform the present membranes closer to the membrane leading-edges. Since evidence so far points towards this possibility, it may be worthwhile to differentiate the arrangement of piezoelectric segments along membrane lengths according to the exact installation type used for the membrane leading-edges to optimise energy harvesting efficiency.

With the availability of membrane outline $y(x)$, the overall harvestable strain energy can be estimated for each Reynolds number according to the following equation [2]:

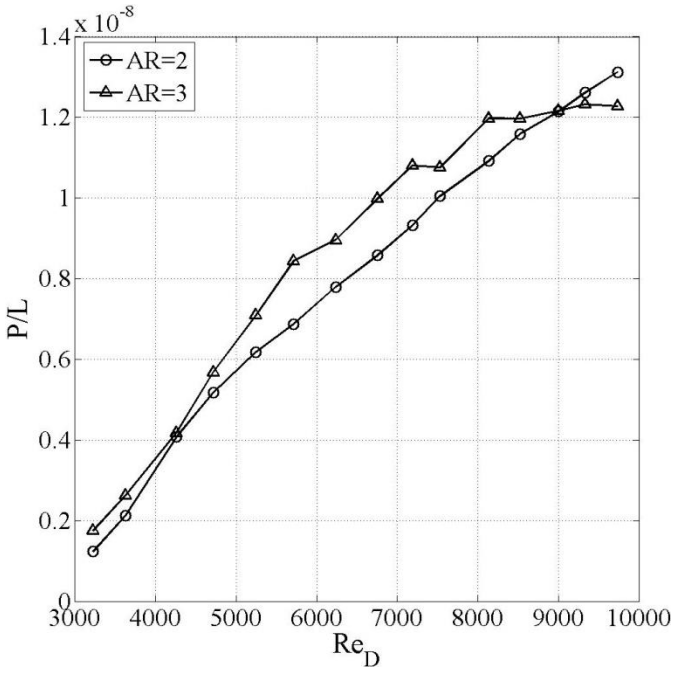

Fig.7 Average strain energy harvested by AR=2 and AR=3 membranes at different Reynolds numbers

$$P = \frac{EI}{2}\int_0^L \frac{(\partial^2 y/\partial x^2)^2}{[1+(\partial y/\partial x)^2]^3} ds \qquad (2)$$

where E is PVDF Young's modulus, I is the second moment of area of the membrane physical geometries, L is the membrane length and s is the curvilinear coordinate. Instantaneous strain energy was calculated according to Eq. 2 by using predetermined membrane outline data, and the final strain energy level for each Reynolds number was obtained by averaging those 11,438 instantaneous strain energy points. Strain energy shown in Fig. 7 was normalised by the membrane length L. Two distinct observations can be made from the figure: Firstly, the increase in the harvestable strain energy with Reynolds number increments is much faster for AR=3 membrane than its AR=2 counterpart. Furthermore, the strain energy growth rate tends to be more linear for the AR=2 membrane. Secondly, the normalised strain energy reaches an asymptotic level from Re_D=8136 onwards, which is shortly after it reaches the "lock-in" state. In

contrast, strain energy of AR=3 membrane continues to grow beyond that particular Reynolds number.

Judging by the evidences consolidated so far, it is reasonable to deduce that for a given set of experimental conditions (i.e. membrane width, membrane installation, Reynolds number and etc), there would be a critical membrane length (hence critical aspect-ratio) above which the strain energy will not increase with the Reynolds number. Increasing the membrane length beyond that associated with the critical aspect-ratio would hasten its approach towards an asymptotic energy-harvesting level due to the increasing presence of strong three-dimensional flapping motions (as shown in Fig. 4).

4. Conclusions

Time-resolved imaging experiments were performed on AR=2 and 3 rectangular PET membranes to study the effects of aspect-ratio on their flapping dynamics. Four main conclusions are arrived at based on quantitative analysis on membrane flapping modes, amplitude, flapping frequency, strain distribution and strain energy. Firstly, despite the fact that the membranes were both seen flapping in Modes A, B and C across the tested Reynolds numbers (Re_D=3228 - 9732), higher aspect-ratio membrane will result in a wider Reynolds number range for Mode C due to its reduced effective stiffness. Membrane flapping amplitude and its growth rate also increases with aspect-ratio, at least for the physical and flow conditions used in the present study. Secondly, membrane aspect-ratio has smaller effects than the Reynolds number on the overall coupling efficacy between the membrane and wake vortices, as indicated by the nearly identical frequency-ratio (i.e. f_m/f_v) growth rates of the two membranes. Similar results were also shown for larger aspect-ratio membranes (i.e. AR=6 and 8) by Allen

and Smits [1]. Thirdly, increasing the membrane aspect-ratio not only alters the distribution of strain peaks, but also appears to impose an upper limit on the maximum strain energy attainable. This is mostly attributed to the heightened three-dimensional flapping motions for AR=3 membrane at high Reynolds numbers, where the coherence level of wake vortices has deteriorated. Therefore, while the AR=3 membrane has a larger strain energy growth rate before approaching its "lock-in" state, it reaches an asymptotic energy-harvesting level earlier than the AR=2 membrane. Lastly, the present results also demonstrate that torsional effects arising from three-dimensional flapping motions should be taken into account in the estimation of the overall harvestable strain energy for large aspect-ratio membranes. For instance, three-dimensional imaging/measurement techniques (e.g. tomographic PIV, Scarano [10]) or three dimensional surface detection methods (Jeon and Sung [11], Adhikari and Longmire [12]) may be used to better discriminate the three-dimensional deformations for better strain energy estimations.

Acknowledgments

The authors gratefully acknowledge the financial support from National Natural Science Foundation of China (Grant Nos.51106096 and 51176108) and Nanyang Technological University Tan Chin Tuan Exchange Fellowship in Engineering for the present study.

References

[1] J.J. Allen, A.J. Smits, Energy harvesting eel, Journal of Fluids and Structures 15 (2001) 629-640.

[2] A.H. Techet, J.J. Allen, A.J. Smits, Piezoelectric eels for energy harvesting in the ocean, in: The Twelfth (2002) International Offshore and Polar Engineering Conference, Kitakyushu, Japan, 2002, pp. 713–718.

[3] W. Taylor, J. Burns, S. Kammann, W. Powers, T. Welsh, The energy harvesting eel: a small subsurface ocean/river power generator, IEEE Journal of Oceanic Engineering 26 (2001) 539–547.

[4] S. Pobering, S. Schwesinger, A novel hydropower harvesting device, in: The 2004 International Conference on MEMS, NANO and Smart Systems, Banff, AL, 2004, pp. 480–485.

[5] N. Elvin, A. Erturk, Advances in Energy Harvesting Methods, Springer, 2013.

[6] Shengxian Shi, T. H. New, Yingzheng Liu, Flapping dynamics of a low aspect-ratio energy-harvesting membrane immersed in a square cylinder wake, Experimental Thermal and Fluid Science 46 (2013) 151-161.

[7] J.E. Mark, Polyer data Handbook, Oxford University Press, 1999.

[8] A. Okajima, Strouhal numbers of rectangular cylinders, Journal of Fluid Mechanics 123 (1982) 379–398.

[9] Y. Jeon, H. Sung, PIV measurement of flow around an arbitrarily moving body, Experiments in Fluids 50 (2011) 787–798.

[10] F. Scarano, Tomographic PIV: principles and practice, Measurement Science and Technology 24 (2013) 012001.

[11] Y. Jeon, H. Sung, Three-dimensional PIV measurement of flow around an arbitrarily moving body, Experiments in fluids 53 (2012) 1057-1071.

[12] D. Adhikari, E. Longmire, Visual hull method for tomographic PIV measurement of flow around moving objects, Experiments in fluids 53 (2012) 943-964.